also be detected by broadening the satellite transitions, a third, sensitive method for probing mobility. The rapid conductivity of these materials means that ^{17}O enrichment is simple and efficient. These new approaches, combined with two-dimensional exchange experiments and with the more traditional relaxation methods for probing dynamics, should yield detailed insight into the mechanisms of conduction in a wide range of oxide conductors.

References and Notes

1. J. B. Goodenough, A. Manthiram, P. Paranthanman, Y. S. Zhen, *Solid State Ionics* **81**, 225 (1992).
2. J. C. Boivin *et al.*, *Solid State Ionics* **113–115**, 639 (1998).
3. J.-C. Boivin, *Int. J. Inorg. Mater.* **3**, 1261 (2001).
4. H. L. Tuller, P. K. Moon, *Mater. Sci. Eng.* **B1**, 171 (1988).
5. Z. Xu, J. F. Stebbins, *Science* **270**, 1332 (1995).
6. S. B. Adler, J. A. Reimer, J. Baltisberger, U. Werner, *J. Am. Chem. Soc.* **116**, 675 (1994).
7. S. Adler *et al.*, *Solid State Ionics* **68**, 193 (1994).
8. F. Wang, C. P. Grey, *Chem. Mater.* **9**, 1069 (1997).
9. ———, *J. Am. Chem. Soc.* **120**, 970 (1998).
10. C. P. Grey, W. S. Veeman, A. J. Vega, *J. Chem. Phys.* **98**, 7711 (1993).
11. C. P. Grey, A. J. Vega, *J. Am. Chem. Soc.* **117**, 8232 (1995).
12. B. Aurivillius, *Ark. Kemi.* **1**, 463 (1949).
13. J. Yan, M. Greenblatt, *Solid State Ionics* **81**, 225 (1995).
14. F. Abraham, M. F. Debreuille-Gresse, G. Mairesse, G. Nowogrocki, *Solid State Ionics* **28–30**, 529 (1988).
15. Y. L. Yang, L. Qiu, W. T. A. Harrison, R. Christoffersen, A. J. Jacobson, *J. Mater. Chem.* **7**, 249 (1997).
16. K. R. Kendall, C. Navas, J. K. Thomas, H. C. z. Loye, *Chem. Mater.* **8**, 642 (1996).
17. R. N. Vannier *et al.*, *Solid State Ionics*, in press.
18. α-$Bi_4V_2O_{11}$ and γ-$Bi_4V_{1.7}Ti_{0.3}O_{10.85}$ were prepared from Bi_2O_3 (99.99%), V_2O_5 (99.99%) and TiO_2 (99.9+%) (Aldrich) by heating at 600°C for 12 hours and at 800°C for 24 hours in a platinum crucible. The sample was then enriched in ^{17}O by heating in $^{17}O_2$ gas (Isotec; minimum 50 atom %) at 800°C for 6 hours. The level of enrichment was estimated to be about 30% on the basis of the volume of gas used. X-ray powder diffraction confirmed the purity of both phases.
19. A. Medek, J. S. Harwood, L. Frydman, *J. Am. Chem. Soc.* **117**, 12779 (1995).
20. S. Yang, K. D. Park, E. Oldfield, *J. Am. Chem. Soc.* **111**, 7278 (1989).
21. G. W. Wagner, *Inorg. Chem.* **30**, 1960 (1991).
22. R. K. Harris, *Nuclear Magnetic Resonance Spectroscopy* (Pitman Books, London, 1983).
23. A. T. Harrison, O. W. Howarth, *J. Chem. Soc. Dalton Trans.* 1953 (1985).
24. N. Kim, C. P. Grey, unpublished data.
25. The effective T_2 (T_2^*) for the individual satellite transitions is $\sim 16(\nu_r/\delta)^2\tau_c$, for random isotropic motion, where δ and ν_r are the correction time for motion, the width of the spectrum, and MAS frequencies, respectively [M. M. Maricq, J. S. Waugh, *J. Chem. Phys.* **70**, 3300 (1979)]. The sidebands are no longer resolved when the linewidths of the spinning sidebands are greater than ν_r. An estimate for $T_2^* < 1/\pi\nu_r$ can then be made from $T_2^* < 1/\pi\nu_r$.
26. F. D. Hardcastle, I. E. Wachs, H. Eckert, D. A. Jefferson, *J. Solid State Chem.* **90**, 194 (1991).
27. I. Abrahams *et al.*, *J. Mater. Chem.* **8**, 1213 (1998).
28. F. Delmaire, M. Rigole, E. A. Zhilinskaya, A. Aboukais, G. Mairesse, *Phys. Chem. Chem. Phys.* **2**, 4477 (2000).
29. This resonance is not ascribed to $BiVO_4$ because the ^{17}O resonances expected for this compound are not observed in the ^{17}O spectrum of α-$Bi_4V_2O_{11}$; however, it is difficult to rule out the total absence of this phase.

30. Support from NSF grant DMR-9901308 is acknowledged. M. Ziliox is thanked for help with the 14.1 T NMR experiments; insightful discussions with R. N. Vannier and G. Mairesse are gratefully acknowledged.

Supporting Online Material
www.sciencemag.org/cgi/content/full/1074130/DC1
Figs. S1 to S3

20 May 2002; accepted 9 July 2002
Published online 18 July 2002;
10.1126/science.1074130
Include this information when citing this paper.

Structural Studies of Several Distinct Metastable Forms of Amorphous Ice

C. A. Tulk,[1]*† C. J. Benmore,[2]* J. Urquidi,[2] D. D. Klug,[3] J. Neuefeind,[2] B. Tomberli,[4] P. A. Egelstaff[4]

Structural changes during annealing of high-density amorphous ice were studied with both neutron and x-ray diffraction. The first diffraction peak was followed from the high- to the low-density amorphous form. Changes were observed to occur through a series of intermediate forms that appear to be metastable at each anneal temperature. Five distinct amorphous forms were studied with neutron scattering, and many more forms may be possible. Radial distribution functions indicate that the structure evolves systematically between 4 and 8 angstroms. The phase transformations in low-temperature liquid water may be much more complex than currently understood.

Amorphous forms of ice have been produced by many techniques. For example, pressurization of ice I to ~13 kbar is known to yield the most common high-density amorphous (HDA) form of ice (*1*). Low-pressure vapor deposition onto a cold target (*2*), rapid quenching of the liquid (*3*), or decompression and heating of the HDA form are known to produce other amorphous forms, all with densities that are similar to that of the crystalline ice I phase. These forms have been categorized as low-density amorphous (LDA) forms. In addition, the LDA form has been reported to abruptly and reversibly transform into the HDA form with the application of pressure, possibly through a first-order phase transition (*4*). This has resulted in the suggestion that all forms of amorphous water can be partitioned into these two high- and low-density forms (*5*). However, a survey of the literature provides the seemingly contradictory view that a continuous range of amorphous structures may exist (*6–10*). In fact, Mishima and others in their original work on the crystalline to amorphous transition stated that "Heating below the 117 K transition causes irreversible changes in the diffraction pattern. . ." (*1*), thus suggesting the possibility of many amorphous forms. However, no detailed structural studies of these possible intermediate forms have ever been reported; therefore, the interpretation of the nature of this important transition is difficult.

Calorimetric studies of this transition have indicated a slow exothermic process followed by a sharp exothermic peak associated with the HDA to LDA transition at 113.4 K at a heating rate of 10 K hour^{-1} (*11*). In addition, subtle differences in the Raman and infrared spectra (*12*, *13*) have been accepted as indicating only minor variations of the more general LDA structural category, and similar claims have been made regarding the HDA category (*7*). Structural studies by neutron and x-ray diffraction (*14–18*) have also resulted in the suggestion that liquid water can be considered a mixture of the low- and high-density forms (*5*). Conversely, relaxation, as indicated by the shift in the first diffraction peak in the HDA form of D_2O upon annealing, has also resulted in the suggestion that some variation in the HDA structure may exist (*7*). Recently, neutron diffraction with isotope substitution experiments on HDA and LDA was also conducted, and the substantial differences in the structures were reported (*19*).

We studied the structural changes during the transition in detail using both neutron and x-ray scattering. We followed the transition continuously by recording the position of the first sharp diffraction peak (FSDP) in the neutron and x-ray static structure factor as a function of time at several anneal temperatures. We found that the

[1]Oak Ridge National Laboratory, Oak Ridge, TN 37831, USA. [2]Argonne National Laboratory, Argonne, IL 60439, USA. [3]National Research Council of Canada, Ottawa, Ontario K0A 0R6, Canada. [4]Department of Physics, University of Guelph, Guelph, Ontario N1G 2W1, Canada.

*These authors contributed equally to this work.
†To whom correspondence should be addressed. Present address: IPNS Division, Argonne National Laboratory, 9700 South Cass Avenue, Argonne, IL 60439, USA.

transition from the high- to the low-density form can occur continuously through a series of amorphous forms that appear to be intermediate and metastable at each anneal temperature over the course of several hours (with every indication that these forms are metastable for much longer times). At each anneal temperature below 110 K, the transition proceeds rapidly at first (possibly through transient structures), but then it becomes kinetically inhibited with no further structural evolution. In all, using neutron diffraction, we studied five metastable amorphous ice forms. We subsequently compared data from each structure at 40 K and, using the derived neutron and x-ray radial distribution functions, identified the major structural changes that occur between each successive metastable form during the HDA to LDA transformation.

HDA ice (99.999% D_2O for neutron studies and 99.99% H_2O for x-ray studies) was formed by pressurizing ice Ih to 18 kbar at 77 K in a piston cylinder apparatus at the National Research Council of Canada. These samples were stored in liquid nitrogen during shipment to Argonne National Laboratory. The neutron diffraction data were collected by using the glass liquids and amorphous materials diffractometer at the Intense Pulsed Neutron Source. Subsections of the samples were placed in a vanadium container and loaded into a precooled cryostat. The loading procedure was carried out at 77 K. The data were analyzed with the ATLAS software package that corrected for background scattering from the empty vanadium can, absorption, and multiple scattering, and the data were normalized to an absolute scale with the isotropic incoherent scattering from vanadium. The resulting differential cross section was then normalized to the high momentum transfer limit (i.e., up to a Q_{max} value of 25 $Å^{-1}$, where Q is the momentum transferred to the sample). This corrected for the unknown effective density of the powdered sample. Finally, the inelastically scattered (Placzek) component was calculated and removed, giving the total neutron static structure factor $S_N(Q)$. Samples used for the x-ray experiments were transferred from liquid nitrogen storage into a cryostat mounted on the high-energy x-ray diffractometer at the 11-ID-C beamline at the Advanced Photon Source (*20*). The sample was loaded into an aluminum holder with thin Kapton film windows. The x-ray measurements were made in transmission geometry with the incident beam energy of 98 keV and scattering from 4-mm-thick samples. The procedure for correcting the data has been outlined in detail (*21*). The x-ray data presented were corrected for detector dead time, container scattering, varying detector distance, and polarization, and they were normalized to the sum of the elastic plus Compton scattering with a Klein-Nishina correction. Multiple scattering and attenuation corrections for this sample were found to be negligible (~1%) at this energy. For both the x-ray and neutron data, the sample temperature was accurate to within ~0.1 K through equilibration with a low-density helium exchange gas in direct contact with the sample. Because the sample was a loosely packed powder and its volume was small (~3 mm by 3 mm by 4 mm for the x-ray experiments and ~5 mm by 5 mm by 6 mm for the neutron measurements) relative to the cold helium exchange gas volume, the thermal gradients within the sample were negligible. The total radial distribution function $G(r)$ is related to the Fiber-Ziman structure factor by the Fourier transform, $S(Q) = 1 + (4\pi\rho/Q)\int r[G(r) - 1]\sin(Qr)dr$, where ρ is the density of the sample in atoms per cubic angstrom. The densities for the HDA and LDA forms were taken from the literature (*1*), and the densities of the quenched intermediate phases were determined by the scaled ratio of the position of the first diffuse peak position to the total peak shift between the HDA and LDA data.

After the samples were loaded at low temperature into the neutron and x-ray diffractometers, they were initially cooled to 40 K, and a data set was collected from the unannealed samples. The fully corrected total x-ray and neutron structure factor functions from the unannealed samples are given in the lower traces of Fig. 1, A and C. The high quality of the samples is demonstrated by the absence of intense crystalline ice Bragg peaks. For the unannealed phases, the first peak position in the neutron structure factor was measured at a momentum transfer of 2.11 $Å^{-1}$; the first peak position in the x-ray structure factor was measured at a momentum transfer of 2.25 $Å^{-1}$. Previously, these peaks had been measured at 2.15 $Å^{-1}$ in both the neutron and x-ray structure factors (*15–17*).

The samples were then annealed at 95, 100, 105, and 110 K for the times specified in Figs. 2 and 3. Structural changes during each isothermal annealing period were partially characterized by recording the position of the FSDP in the structure factor. After some time, no further structural evolution was apparent (i.e., when the slope of the curves through the FSDP position as a function of time is zero), therefore suggesting that a metastable structure had formed at each anneal temperature. The temperature was then reduced to 40 K for comparison of the $S(Q)$ functions among amorphous forms. The temperature was then increased for the next iso-

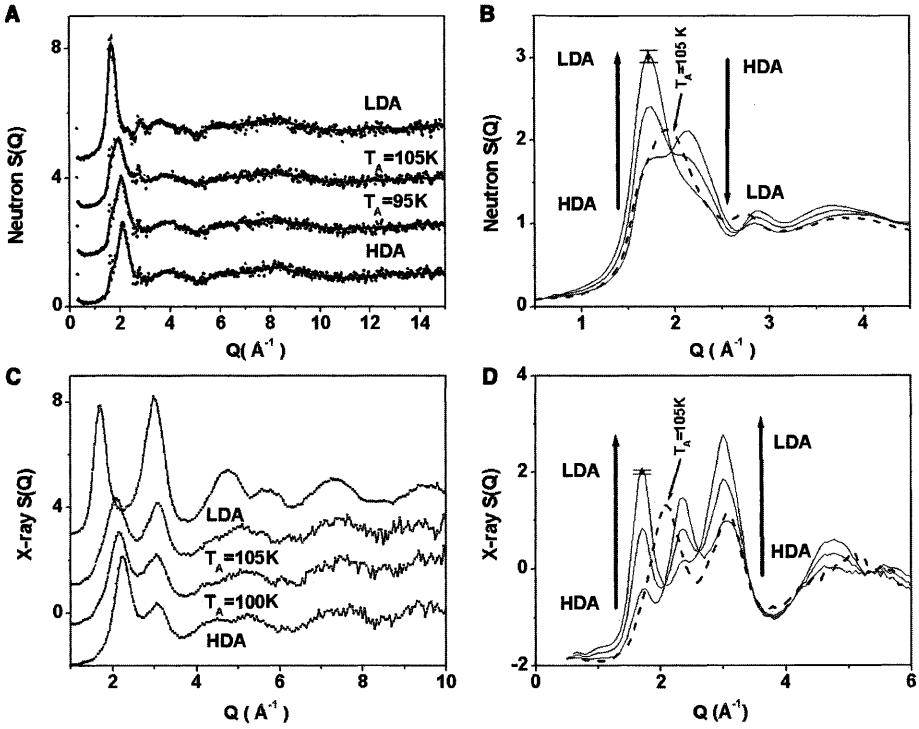

Fig. 1. (**A**) Total neutron $S(Q)$ from D_2O and (**C**) x-ray $S(Q)$ from H_2O of several amorphous ice forms. Data were recorded at T = 40 K after each anneal. Neutron data sets were collected for 12 hours, and x-ray data sets were collected for 3 hours. Solid lines in (A) are the smoothed functions. These data were used to obtain the radial distribution functions plotted in Fig. 4 (where Q_{max} = 25 $Å^{-1}$). Linear combinations $[xS_{HDA}(Q) + (1 - x)S_{LDA}(Q)]$ of the (**B**) neutron and (**D**) x-ray structure factors are also presented. The arrows indicate the trend from HDA to LDA, and the values of x were taken to be 0.75, 0.50, and 0.25. Superimposed on these curves is the measured $S(Q)$ after annealing at 105 K (dashed curve). The annealed structure is unique and cannot be represented by any combination of LDA and HDA. The error in $S(Q)$ at Q = 1.7 $Å^{-1}$ for the x-ray data is ±1% and for the neutron data is ±2.4% (see representative error bars on plots).

thermal annealing cycle. Several of the neutron and x-ray $S(Q)$ functions collected at 40 K are shown in Fig. 1.

The FSDP positions in the neutron $S(Q)$ are given as a function of total anneal time for each isothermal anneal temperature in Fig. 2, and those from the x-ray $S(Q)$ are given in Fig. 3. The temperature dependence of the neutron FSDP was measured and shown to change from 1.95 ± 0.02 to 1.93 ± 0.02 Å^{-1} upon cooling from 105 to 40 K. Therefore, temperature and thermal expansion can be excluded as a possible cause of the peak shift in these plots. These data indicate that there are no sharp discontinuities in the peak position during the transformation, and thus we conclude that, at the local structure level, amorphous ice can evolve continuously from the high- to the low-density form. During the 110 K anneal, the sample overcomes the remaining potential barriers, and the structure evolves toward the lowest density, or LDA, structure. We note that the structure after an isothermal anneal, at any given anneal temperature, may not be identical from sample to sample. This is because the transition is highly exothermic, and therefore the degree of structural evolution may depend on the packing morphology and the efficiency of the heat transport mechanism (i.e., low-pressure helium exchange gas in this case); these conditions are very difficult to reproduce from experiment to experiment. Furthermore, if the heat removal mechanism is not sufficiently efficient, the transition may continue to the LDA form and thus appear to occur through a series of transient rather than metastable amorphous forms.

In addition to the unannealed HDA and final LDA form, three other distinct intermediate forms were studied at 40 K with neutron diffraction. In the neutron $S(Q)$ in Fig. 1A, the FSDP progresses toward lower momentum transfer with increasing anneal temperature, from 2.11 to 2.06 to 1.92 and finally to 1.67 Å^{-1} in the LDA phase. This is accompanied by an increasing peak intensity (atom–atom correlations) at ~2.85 Å^{-1} and a shift to lower momentum transfer of the broad peak seen from 4.0 to 3.63 Å^{-1}. The x-ray structure factor, in Fig. 1C, shows a similar trend; the FSDP position also shifts toward lower momentum transfer, from 2.25 to 2.16 to 2.09 and finally to 1.71 Å^{-1}, for the phases shown. Also shown is an initial decrease in the x-ray FSDP intensity, followed by an increase in intensity and substantial sharpening in the final LDA phase. This is accompanied by a sizable increase in the intensity of the peaks at 3.05 and 4.75 Å^{-1}. The general features of both the unannealed HDA and the final LDA structure factors from x-ray and neutron scattering agree very well with those recorded previously (*15–17*), with, however, the exception of the intensity of the second peak in the reported x-ray HDA $S(Q)$ measurement (*15*), which is closer to that measured in the LDA form. This may indicate that the previously measured x-ray $S(Q)$ could have resulted from a partially annealed HDA structure. Careful evaluation of the data showed that the $S(Q)$ functions from each intermediate form are distinct; that is, they cannot be reproduced by any linear combina-

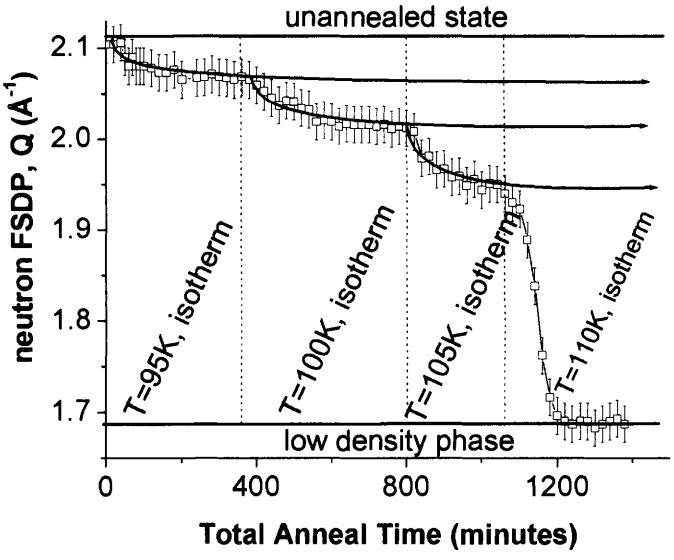

Fig. 2. The position of the FSDP in the neutron structure factor as a function of total anneal time. After each isothermal anneal, the samples were cooled to 40 K for structural comparison (see Fig. 1). The unannealed state corresponds with the HDA phase. The solid curves were drawn to aid the eye. Pressurization of ice I at lower temperatures will probably result in a slightly different structure.

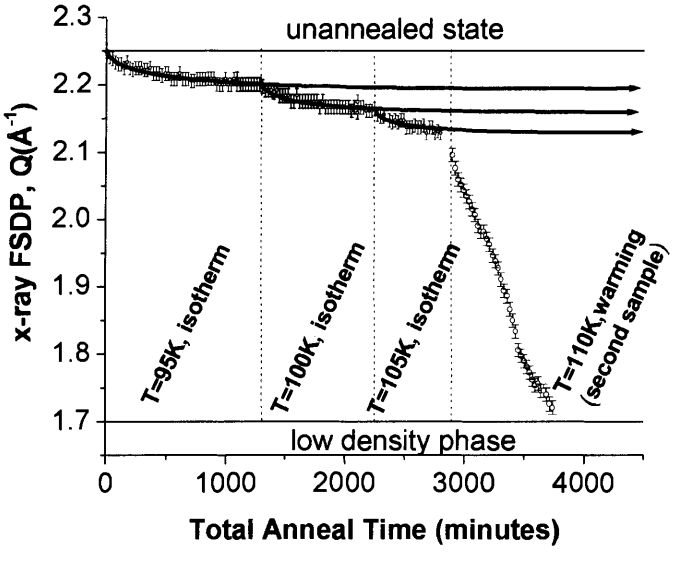

Fig. 3. The position of the FSDP in the x-ray structure factor as a function of total anneal time. The results from two samples are plotted. Data from the second sample are indicated after 3000 min during transformation to the low-density form after warming above 110 K. The solid horizontal lines represent the measured position of the first diffraction peak in the high-density form and the low-density form. As with the neutron data, the structures were cooled to 40 K after each anneal structural comparison. The solid curves are drawn to aid the eye.

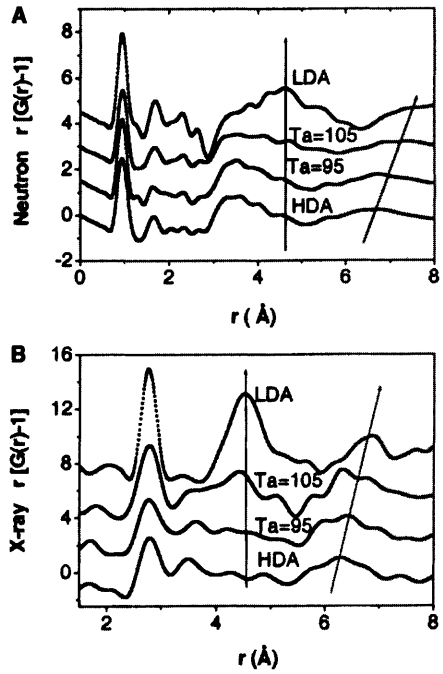

Fig. 4. (**A**) The neutron radial distribution functions and (**B**) the x-ray radial distribution functions calculated from data presented in Fig. 1. The densities used in the transforms were 0.1174, 0.1146, 0.1078, and 0.09434 atoms Å^{-3} for the progression from HDA to LDA in the neutron scattering case and 0.1174, 0.1110, 0.1107, and 0.09434 atoms Å^{-3} for the x-ray scattering experiments.

tion of the HDA and LDA $S(Q)$ functions. Several combinations of the $S(Q)$ of the HDA and LDA structures are plotted in Fig. 1, B (neutron data) and D (x-ray data); also plotted are the data from the sample annealed at 105 K. The annealed structures factors cannot be produced by any combination of LDA and HDA. We note the region in Fig. 1D where the x-ray curves intersect at 2.05 $Å^{-1}$, the peak is at 2.09 $Å^{-1}$ for the annealed sample, and there is only a small error in the data in this region.

The measured total structure factors of the quenched states were transformed into real-space radial distribution functions, and the several representative data sets are plotted in Fig. 4A for the neutron experiments and in Fig. 4B for the x-ray experiments. Although the neutron data are predominantly weighted toward the hydrogen–hydrogen and oxygen–hydrogen correlations and the x-ray data are predominantly weighted toward the oxygen–oxygen correlations, the major real-space structural trends upon annealing can be seen in both sets of data, and they are generally described by short- to intermediate-range structural changes between 4 and 8 Å. The broad peak centered on ~6.4 Å shifts systematically to greater distance with increasing anneal temperature. In addition, a substantial increase in the intensity of the broad peak centered at ~4.5 Å with increasing anneal temperature is noted. The hydrogen-bonded oxygen–oxygen distance, given by the position of the first peak in the x-ray $G(r)$, shortens systematically through the transformation between each amorphous form and ranges from 2.80 Å in the unannealed HDA phase to 2.76 Å in the final lowest density phase; this is consistent with measured Raman data (*23*).

We annealed HDA ice at several temperatures below 113.4 K (i.e., the recorded transition temperature to the LDA form). It is seen from the position of the FSDP in the static structure factor that the transition from the HDA form to the LDA form can proceed in a structurally continuous manner through a series of intermediate, apparently metastable amorphous forms. Several of these metastable forms were observed, and detailed radial distribution functions were compared at temperature $T = 40$ K. It is reasonable to expect that, in principle, a continuous distribution of recoverable forms between HDA and LDA ice is possible. At any $T < 113.4$ K, the thermal energy is insufficient to overcome the potential barriers that define a particular metastable structure. This is what is in general expected for the existence of any metastable phase and indicates that the transformation between the poly-amorphs of ice may be somewhat complex. From the radial distributions functions presented here, it appears that the transition predominantly evolves on the short to intermediate length scale; that is, major structural changes occur between 4 and 8 Å, and more subtle changes also occur on the hydrogen bond length scale. These data may have important implications regarding the current understanding of the structural relation between a low-density liquid water and LDA ice, and a high-density liquid water and HDA ice (*2*, *23*–*25*). These results may also impact on the character of the transformation from ice Ih to HDA (*5*, *26*), the HDA-LDA mixture model (*5*), and the relations between normal water and HDA. In addition, understanding structural variations in amorphous water, particularly the predominant length scales over which such variations occur, may provide a basis for understanding biomolecular hydration and cryopreservation.

References and Notes

1. O. Mishima, L. D. Calvert, E. Whalley, *Nature* **310**, 393 (1984).
2. E. F. Burton, W. F. Oliver, *Proc. R. Soc. London Ser. A* **153**, 166 (1936).
3. E. Mayer, *J. Appl. Phys.* **58**, 663 (1985).
4. O. Mishima, *J. Chem. Phys.* **100**, 5910 (1994).
5. ———, H. E. Stanley, *Nature* **396**, 329 (1998).
6. E. Whalley, O. Mishima, Y. P. Handa, D. D. Klug, *Ann. N.Y. Acad. Sci.* **484**, 81 (1986).
7. H. Schober *et al.*, *Physica B* **241–243**, 897 (1998).
8. G. P. Johari, A. Hallbrucker, E. Mayer, *Science* **273**, 90 (1996).
9. T. Loerting, C. Salzmann, I. Kohl, E. Mayer, A. Hallbruker, *Phys. Chem. Chem. Phys.* **3**, 5355 (2001).
10. O. Mishima, *Nature* **384**, 546 (1996).
11. Y. P. Handa, O. Mishima, E. Whalley, *J. Chem. Phys.* **84**, 2766 (1986).
12. C. A. Tulk, D. D. Klug, R. Branderhorst, P. Sharpe, J. A. Ripmeester, *J. Chem. Phys.* **109**, 8478 (1998).
13. E. Mayer, *J. Phys. Chem.* **89**, 3474 (1985).
14. M. A. Floriano, E. Whalley, E. Svensson, V. F. Sears, *Phys. Rev. Lett.* **57**, 3062 (1986).
15. A. Bizid, L. Bosio, A. Defrain, M. Oumezzine, *J. Chem. Phys.* **87**, 2225 (1987).
16. M. C. Bellissent-Funel, J. Teixeira, L. Bosio, *J. Chem. Phys.* **87**, 2231 (1987).
17. M. C. Bellissent-Funel, L. Bosio, A. Hallbruker, E. Mayer, R. Sridi-Dorbez, *J. Chem. Phys.* **97**, 1282 (1992).
18. L. Bosio, G. P. Johari, J. Teixeira, *Phys. Rev. Lett.* **56**, 460 (1986).
19. J. L. Finney, A. Hallbrucker, I. Kohl, A. K. Soper, D. T. Bowron, *Phys. Rev. Lett.* **88**, 225503 (2002).
20. U. Rütt *et al.*, *Nucl. Instrum. Methods A* **467**, 1026 (2001).
21. B. Tomberli, C. J. Benmore, P. A. Egelstaff, J. Neuefeind, V. Honlimaki, *J. Phys. Condens. Matter* **12**, 2597 (2000).
22. D. D. Klug, O. Mishima, E. Whalley, *J. Chem. Phys.* **86**, 5323 (1987).
23. M.-C. Bellissent-Funel, *Europhys. Lett.* **42**, 161 (1998).
24. F. W. Starr, M.-C. Bellissent-Funel, H. E. Stanley, *Phys. Rev. E* **60**, 1084 (1999).
25. A. K. Soper, M. A. Ricci, *Phys. Rev. Lett.* **84**, 2881 (2000).
26. J. S. Tse *et al.*, *Nature* **400**, 647 (1999).

27. Supported by the U.S. DOE contract nos. DE-A05-00R22725 and W-31-109-ENG-38.

20 May 2002; accepted 11 July 2002

The Vibration-Rotation Emission Spectrum of Free BeH_2

Peter F. Bernath,[1]* Alireza Shayesteh,[1] Keith Tereszchuk,[1] Reginald Colin[2]

The gaseous BeH_2 molecule has been synthesized by means of an electrical discharge inside a high-temperature furnace and identified with infrared emission spectroscopy. The antisymmetric stretching mode ν_3 has been detected near 2179 reciprocal centimeters. The BeH_2 molecule has a linear, symmetric structure with an r_0 BeH bond length of 1.333761(2) angstroms.

With only six electrons, BeH_2 is a favorite target molecule for testing new ab initio quantum chemical methods [for example, (*1*–*4*)]. Despite this strong interest in BeH_2, the free molecule remains unknown. It has been detected previously through its infrared spectrum when stabilized in an argon matrix at 10 K (*5*), or in a silicon crystal as an impurity (*6*). Although solid BeH_2 is well known (*7*), this material is in fact based on a three-dimensional arrangement of connected BeH_4 tetrahedra (*8*).

[1]Department of Chemistry, University of Waterloo, Waterloo, Ontario N2L 3G1, Canada. [2]Laboratoire de Chimie Physique Moléculaire, Université Libre de Bruxelles, C.P. 160/09, 50 avenue F. D. Roosevelt, 1050 Brussels, Belgium.

*To whom correspondence should be addressed. E-mail: bernath@uwaterloo.ca

Heating BeH_2 solid results in decomposition to the elements, not the production of BeH_2 vapor. The insertion of ground-state Be atoms into the H_2 bond is predicted (*9*) to have an activation barrier of 203.5 kJ/mol (48.6 kcal/mol), whereas the overall reaction

$$Be(g) + H_2(g) \rightarrow BeH_2(g)$$

is predicted (*10*) to be favorable and to be exoergic by 157.3 kJ/mol (37.6 kcal/mol). BeH_2 is calculated (*11*) to be linear and to have a bond length of 1.3324 Å, close to the observed value of 1.3417 Å for the BeH free radical (*12*).

We now report the formation of BeH_2 with an emission source that allows an electrical discharge inside a high-temperature furnace and the characterization of BeH_2 by infrared (IR) emission spectroscopy (*13*). The central part of